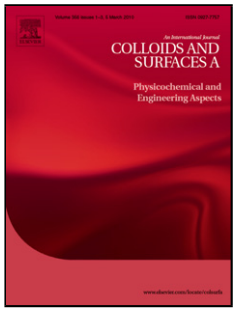

Title: Characterization of *Skeletonema costatum* Intracellular Organic Matter and Study of Nanomechanical Properties under Different Solution Conditions

Author: Leonardo Gutierrez Cyril Aubry Laure Dramas Pierre Aimar Jean-Philippe Croue

PII: S0927-7757(16)30467-8
DOI: http://dx.doi.org/doi:10.1016/j.colsurfa.2016.06.025
Reference: COLSUA 20752

To appear in: *Colloids and Surfaces A: Physicochem. Eng. Aspects*

Received date: 27-3-2016
Revised date: 15-6-2016
Accepted date: 16-6-2016

Please cite this article as: Leonardo Gutierrez, Cyril Aubry, Laure Dramas, Pierre Aimar, Jean-Philippe Croue, Characterization of Skeletonema costatum Intracellular Organic Matter and Study of Nanomechanical Properties under Different Solution Conditions, Colloids and Surfaces A: Physicochemical and Engineering Aspects http://dx.doi.org/10.1016/j.colsurfa.2016.06.025

Characterization of *Skeletonema costatum* Intracellular Organic Matter and Study of Nanomechanical Properties under Different Solution Conditions

Submitted to

COLLOIDS AND SURFACES A: PHYSICOCHEMICAL AND ENGINEERING ASPECTS

March 2016

Leonardo Gutierrez[1, 2], Cyril Aubry[3], Laure Dramas[4], Pierre Aimar[5], and Jean-Philippe Croue[1, 4*]

[1] Curtin Water Quality Research Centre, Department of Chemistry, Curtin University, Australia

[2] Facultad del Mar y Medio Ambiente, Universidad del Pacifico, Guayaquil, Ecuador

[3] Masdar Institute of Science and Technology, Abu Dhabi, United Arab Emirates

[4] Water Desalination and Reuse Center, King Abdullah University of Science and Technology, Saudi Arabia

[5] University of Toulouse, Toulouse, France

* Corresponding author: Tel.: +61 (0) 8 9266 9793
E-mail address: jean-philippe.croue@curtin.edu.au

25 pages and 6 figures are included in the current manuscript.

Graphical Abstract

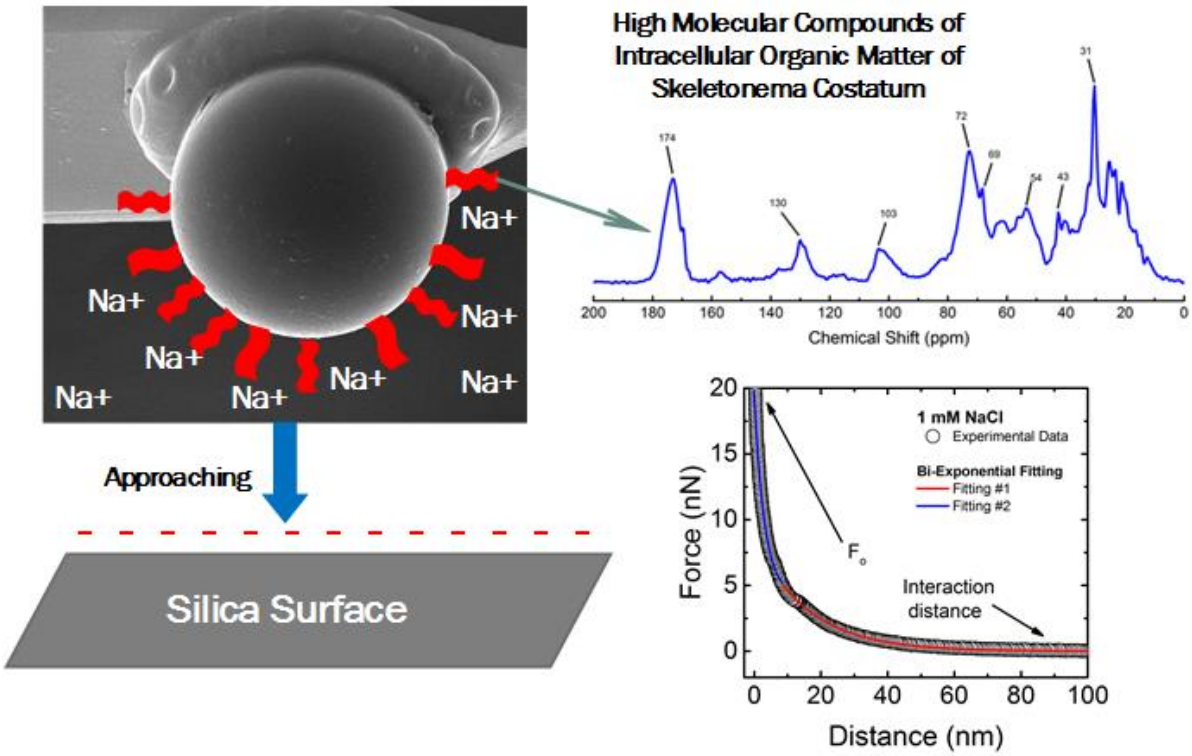

Highlights

- Models of polymer physics were applied to describe HMW SKC-IOM polymeric nature
- HMW SKC-IOM polymeric structure showed highly responsive to solution chemistry
- Two regions of different nanomechanical properties were observed in HMW SKC-IOM
- HMW SKC-IOM showed fully extended chains at low ionic strength
- HMW SKC-IOM evidenced compressed structures with increasing salt concentration

Abstract

In the current investigation, a rigorous characterization of the high molecular weight (HMW) compounds of *Skeletonema costatum* (SKC) intracellular organic matter (IOM), including nanomechanical properties, was conducted. HMW SKC-IOM was characterized as a mixture of polysaccharides, proteins, and lipids. Atomic force microscopy (AFM) provided crucial information of this isolate at a nanoscale resolution. HMW SKC-IOM showed highly

responsive to solution chemistry: fully extended chains at low ionic strength, and compressing structures with increasing electrolyte concentration in solution. Interestingly, two regions of different nanomechanical properties were observed: a) Region #1: located farther from the substrate and showing extended polymeric chains, and b) Region #2: located <10 nm above the substrate and presenting compressed structures. The polymer length, polymer grafting density, and compressibility of these two regions were highly influenced by solution conditions. Results suggest that steric interactions originating from HMW SKC-IOM polymeric structure would be a dominant interacting mechanism with surfaces. The current investigation has successfully applied models of polymer physics to describe the complex HMW SKC-IOM structural conformation at different solution conditions. The detailed methodology presented provides a tool to characterize and understand biopolymers interactions with surfaces, including filtration membranes, and can be extended to other environmentally relevant organic compounds.

Keywords: Atomic force microscopy; Organic matter; nanomechanical properties; Skeletonema Costatum; Interfacial interactions.

1. Introduction

Several regions in the world are currently experiencing a lack of water resources to meet the demands of a growing global population. This water demand has constantly increased because of the expansion and development of urban areas, industries, and agriculture; consequently resulting in water scarcity (i.e., water stress, shortage, or crisis) [1]. In addition, the unsustainable use of freshwater has significantly affected the quality and quantity of this resource, exacerbating environmental problems. During the last decades, seawater desalination has emerged as a suitable option for those regions (e.g., Middle East, Australia, and Europe)

with intense freshwater use or limited (i.e., or even depleted) freshwater resources [2]. Nevertheless, the occurrence of episodic marine algal bloom events represents a major drawback that significantly affects the performance of desalination plants (i.e., increased membrane fouling rates and operational costs) [3, 4]. For instance, in 2008 Arabian Gulf countries (i.e., highly dependent on desalination plants as their main source of freshwater) shut down water production due to a *Cochlodinium polykrikoides* bloom [2, 5]. Interestingly, the frequency, intensity, and geographic distribution of algae blooms have increased in the last decades.

During a marine algae bloom, the microscopic planktonic algae rapidly proliferate and can reach concentrations of several hundred thousand cells/mL [3]. These algae blooms usually occur at the seawater surface and in coastal areas, thus impacting human activities [6]. In addition to coloration of water, release of toxins, and production of taste or odor compounds; marine algae blooms generate turbidity and high concentrations of algal organic matter (i.e., AOM-referring to a wide range of macromolecules such as oligosaccharides, amino acids, lipids, polysaccharides, proteins, or peptides) [4, 7]. This large AOM content, originated from algal biomass (i.e., intracellular organic matter–IOM, generated inside the cell and released during lysis) and the production of extracellular organic matter (i.e., EOM, excreted by algal cells during growth), causes high and even irreversible fouling in desalination systems [3, 4].

To advance our knowledge of AOM impact on desalination processes, numerous approaches for characterizing and identifying recalcitrant AOM foulant fractions have been developed and comprehensively studied. Briefly, Liquid Chromatography coupled with Organic Carbon Detector and UV Detector at 254 nm (LC-OCD) analysis has been conducted on different algal monocultures (e.g., *Alexandrium tamarense, Chaetoceros affinis, Microcystis sp., Scenedesmus sp.*, etc.) [8-10]. Although different fractions could be detected from the LC-OCD profiles (i.e., biopolymer peaks, aromatic fractions, low molecular weight neutrals, etc.),

hydrophilic compounds were present as the dominant fraction for all phases of growth (i.e., IOM and EOM, contributing to >50% of the total organic carbon - TOC). Similarly, Fourier Transform Infra-Red spectroscopy (FTIR) analyses have confirmed the strong presence of carbohydrate-like and protein-like compounds in AOM. ^{13}C-Nuclear Magnetic Resonance (^{13}C-NMR) technique has been used in AOM samples of different sizes (i.e., ranging from 1 kDa to 1.6 μm) and has also confirmed the complex nature of AOM as mainly composed by a mixture of carbohydrates and proteins [11-13]. In addition, Pyrochromatograms of AOM (Pyrolysis-Gas Chromatography coupled with Mass Spectroscopy - Pyrolysis-GC-MS) have shown the presence of pyrroles and nitriles (i.e., produced from the pyrolysis of proteins and nucleic acids, respectively), furans (polysaccharides by-products), and phenols (i.e., resulting of the thermal degradation of lignin, polycarboxylic acids, or proteins) [13-15]. In contrast, Fluorophore regions and Fluorescence Emission Excitation Matrices (FEEM) of different AOM samples have indicated the presence of marine humic-like substances during growth in EOM and its absence in the IOM matrix, suggesting excretion [16].

Recently, Atomic Force Microscopy (AFM) has been introduced as a versatile tool to characterize different AOM fractions and algae cells. Briefly, AFM was used to image and analyze macromolecular structures of various carrageenan types extracted from red algae of *Gigartinaceae* and *Tichocarpaceae* families, and the surface morphology of *M. aeruginosa*-fouled PVC membrane [17, 18]. In addition, force measurements between a silicon nitride AFM tip and *Enteromorpha linza* were conducted to obtain mechanical properties of the hydrated spores (i.e., Young's modulus, maximum adhesion forces, and maximum adhesion distance) [19]. Likewise, in a previous comprehensive study, adhesion forces between AOM-coated AFM probe and polyethersulfone (PES) membrane or AOM-fouled PES membrane were measured to investigate the tendency of AOM to adsorb to surfaces and to AOM

compounds (i.e., extracted from *Alexandrium tamarense, Chaetoceros affinis,* and *Microcystis sp.*) [10].

The target of this study is to build upon these previous investigations for obtaining a correlation between the physicochemical characteristics and nanomechanical properties of AOM (i.e., analysis of the polymeric nature of AOM). This nano-scale understanding represents a gap in knowledge and would highly contribute to: a) understand biopolymers conformational change with solution conditions and their respective interactions with surfaces (i.e., with specific implications to membrane filtration), and b) to provide a rational basis to the optimization of membrane surface characteristics/properties in desalination systems. For the current study, the High Molecular Weight (HMW) structures (i.e., biopolymers) of IOM of *Skeletonema costatum* (i.e., SKC-a ubiquitous seawater algae responsible for algal bloom [20]) were selected as model AOM (i.e., the HMW compounds of SKC-IOM have been identified as a major foulant for ceramic and polymeric membranes [21]) and rigorously characterized using Elemental Analysis, FTIR, Pyrolysis-GC-MS, ^{13}C-NMR, and ^{1}H-NMR. In addition, the nanomechanical properties (i.e., polymer length, polymer grafting density, compressibility, and decay length) of this HMW SKC-IOM were studied at different solution chemistries by AFM and mathematically described by models of polymer physics.

2. Materials and Methods

2.1. Algae species and Culture Protocol

Skeletonema costatum (SKC) was selected as a model algae strain for this project (i.e., provided by the Oceanographic Observatory of Banyuls-sur-Mer, ARAGO, France). Seawater was collected at the Red Sea, filtered through a 0.45 μm membrane, and then stored in the dark until use. Culture media was prepared by adding nutrients (F/2 Guillard) to the seawater sample (10 liters). This solution was autoclaved at 120°C for 20 minutes and then allowed to cool down for further SKC inoculation. SKC culture was exposed to artificial light 12 hours a day for 6

weeks, where the temperature was kept at 18°C. Every two weeks, a new inoculation process (in 50 mL tubes) was conducted to maintain the SKC culture at an exponential phase of growth. Additionally, aeration with ambient air was continuously provided to prevent algae sedimentation and to allow an efficient air exchange and exposition to light for all cells.

2.2. Isolation of High Molecular Weight Compounds of SKC-IOM

To separate SKC cells, at the decline phase of growth (approximately 20 days of culture) 8 L of culture solution was centrifuged at 3000 g for 15 min. The supernatant was carefully removed, and the resulting pellet (SKC cells) was re-suspended, sonicated (QSONICA Q700, Hielscher, Germany) at 350 Watts for 10 minutes, and filtered through 0.7 μm. This final solution contained the Intracellular Organic Matter (IOM) of SKC. The High Molecular Weight (HMW) compounds of SKC-IOM were obtained through a 3.5 kDa dialysis process (i.e., retained inside the dialysis bag) against MilliQ water (Millipore, USA). The MilliQ water was changed every two days until reaching a permeate conductivity below 10 μS/cm. Samples of HMW SKC-IOM were collected and freeze-dried for analytical purpose. An additional characterization of: filtered/centrifuged SKC culture solution, SKC-IOM, and HMW SKC-IOM by Liquid Chromatography-Organic Carbon Detection (LC-OCD) was conducted to assess the isolation protocol efficiency, and it is described in the Supplementary Data section.

2.3. Characterization of the High Molecular Weight compounds of SKC-IOM

HMW SKC-IOM was characterized using the following solid-state analytical tools. For Attenuated Total Reflectance–Fourier Transform Infrared Spectroscopy (ATR-FTIR) analyses, the potassium bromide (KBr) pellet method was used. Briefly, KBr pellets were prepared by mixing and grinding 0.3 mg of dried sample with 100 mg of KBr salt. Transparent and thin pellets of approximately 0.5 mm in thickness were formed by subjecting the mixture to a press at 10 tons/inch^2. The HMW SKC-IOM sample was mixed with analytical grade KBr. A blank sample containing only KBr was measured prior to analyses and used to remove background

noise. The wavelength of the generated spectra ranged from 400 cm^{-1} to 4000 cm^{-1}. Solid-state ^{13}C-NMR spectra were acquired with a Bruker AVANAC III 400 MHz spectrometer equipped with a triple-resonance 4 mm Bruker MAS probe. ^{13}C-Cross Polarization-Magic Angle Spinning-NMR (^{3}C-CP-MAS-NMR) spectra were acquired at a resonance frequency of 100.622 MHz under a 14 kHz spinning rate. Bruker Topspin 3.0 software was used for data collection and for spectral analysis. Electrophoretic mobility (EPM) of HMW SKC-IOM or silica particles (1.6 μm in diameter, PolySciences, USA) were measured by a ZS ZEN3600 Zetasizer (Dispersion Technology Software v5.10, 2008, Malvern, UK) using 1 mL clear disposable zeta cells (DTS1060C, Malvern, UK) at pH 5.8±0.1 under the following ionic strength: 1, 3, 10, 30, and 100 mM NaCl. Silica particles were coated with HMW SKC-IOM by the layer-by-layer procedure using positively-charged iron oxide as an intermediate layer, as described elsewhere [22]. A minimum of three replicate solutions per electrolyte condition were prepared and measured. The EPM values obtained were converted to zeta potentials by the Smoluchowski equation. The characterization protocol of HMW SKC-IOM by Pyrolysis-GC-MS, ^{1}H-NMR, and elemental analysis is described in the Supplementary Data section.

2.4. Measurement of interaction forces between HMW SKC-IOM and silica surface

Interaction forces between HMW SKC-IOM and silica wafer (i.e., selected as a model smooth surface) were measured with a 5500 Scanning Probe Microscope (5500 SPM, Agilent Technologies, USA) [23]) Colloidal AFM probes were prepared by gluing a 20 μm silica sphere on a silicon nitride cantilever (SICON, AppNano, USA). The diameter of the silica sphere was measured by Scanning Electron Microscopy (SEM Quanta 3D-FEG, FEI, Netherlands). The sensitivity of the cantilevers were first determined. The spring constant of the cantilevers were obtained by the Thermal Tuning method, while the deflection (V) was converted to force (nN) in accordance to Hooke's law [23]. The HMW SKC-IOM coating procedure of the AFM probe was conducted following the layer-by-layer procedure using iron

oxide as an intermediate layer as described elsewhere [24-28]. Briefly, the AFM colloidal probe was immersed in a previously prepared iron oxide solution for 8 h (i.e., precipitation of iron oxide was performed by increasing the pH of a 10 mM $FeCl_3$ solution to 7 by small additions of NaOH). The iron oxide-coated AFM probe was removed from the iron oxide solution and then immersed in MilliQ water. After careful rinse, the probe was immersed in 300 μL of a 100 mg C/L HMW SKC-IOM solution and allowed to coat for another 8 h. The HMW SKC-IOM-coated AFM probe was again carefully rinsed in MilliQ water and immediately used for experimentation. The successful HMW SKC-IOM coating of the AFM colloidal probes was evidenced by SEM micrographs as previously described [25] (i.e., HMW SKC-IOM-coated AFM probes subjected to SEM were not used for experimentation). Approaching and retracting force profiles were acquired at a 400 nm/s rate (Pico View v.1.8.2 software, Agilent Technologies, USA) [29]. The force load was carefully controlled and set in preliminary experiments to prevent damage to the polymeric structures of the HMW SKC-IOM coating layer during interactions with silica surface. The selected solution chemistries for the current AFM study were: 1, 3, 10, 30, and 100 mM NaCl at a pH 5.8±0.1. A minimum of 40 force vs distance profiles per solution condition were obtained at different locations of the silica surface. AFM experiments were conducted by duplicate with different HMW SKC-IOM-coated AFM probes for reproducibility purposes. In addition, SEM micrographs of HMW SKC-IOM-coated AFM probes after experimentation were acquired to assess the HMW SKC-IOM coating completeness of the AFM probes. The generated force vs distance profiles were processed, analyzed, and modeled as described in the following section.

2.5. AFM data reduction and description by models of polymer physics

Approaching force curves were individually and rigorously analyzed for the following parameters: decay length, interaction distance, polymer grafting density, compressibility, and polymer length. Briefly, interaction force decay length (κ^{-1}) was calculated based on the

repulsive force profile following an exponential decay. Decay length was described by the equation: $F=F_0 \bullet \exp(-\kappa d)$ (i.e., F: interacting force, F_0: pre-exponential constant, d: separation distance). The values of decay length obtained at different ionic strength were further compared to theoretical Debye length [30]. To further investigate the nature of the repulsive forces between HMW SKC-IOM and silica surfaces, the approaching for profiles were fitted by the Alexander-de Gennes model and described by the formula: $F=50k_bTRL_0\Gamma^{3/2}\exp[-2\pi(d/L_0)]$ (i.e., F: interacting force, k_b: Boltzmann's constant, T: temperature, R: AFM probe radius, d: separation distance) [31]. Polymer length (L_0) and polymer grafting density (Γ) were determined as the fitting parameters. This equation considers steric interactions between surfaces caused by the presence of a grafted polymer layer in a good solvent. The compressibility of HMW SKC-IOM polymeric structures (in units of N/m^2) was calculated as the gradient of the slope of the force-displacement curve between the point of contact (i.e., interaction distance between the organic sample and silica surface in contact regime) and the region of constant compliance (i.e., linear response of the AFM tip) [19, 23]. Additionally, a rigorous statistical analysis by probability density functions were conducted the resulting parameters (i.e., decay length, interaction distance, F_0, etc.) to obtain their mean (μ) and sigma (σ). Finally, classic Derjaguin-Landau-Verwey-Overbeek (DLVO) theory of colloid stability was used to calculate theoretical energy barriers arising between HMW SKC-IOM-coated probe and silica surface (i.e., sphere-plate model) as the sum of the Lifshitz-van der Waals and electrostatic double-layer interactions (i.e., zeta potentials were used as an approximation to the electrostatic surface potential of the interacting surfaces) [30, 32, 33]. However, classic DLVO theory has been marginally successful describing interaction between organics or biological systems (i.e., DLVO theory is valid for perfectly smooth surfaces). Deviations from DLVO theory would provide evidence of the presence of specific interactions.

3. Results and Discussion

3.1. Structural properties of HMW-SKC-IOM

FTIR analysis allowed to highlight the predominant structural features of HMW SKC-IOM (Figure 1). The identification of infrared (IR) absorption peaks was conducted following the protocol previously described [13]. Specifically, the strong adsorption band at 3400 cm^{-1} is characteristic of hydrogen bonding. In addition, amide-A (3294 cm-1), amide-B (3090 cm-1), amide-I (1650 cm-1), amide-II (1555 cm^{-1}), and amide-III (1410 cm^{-1}) signals were assigned to proteins. The presence of polysaccharides/sugars was observed through the detection of a broad band near 1037 cm^{-1} (i.e., stretching vibration of C-O). A sharp peak at 1384 cm^{-1} (i.e., symmetric bending vibration of CH_3 of N-acetyl group) along with amide-I and amide-II peaks, and sugar bands, are characteristic of N-acetyl aminosugars (i.e., degradation product of bacterial cell wall peptidoglycans) [13]. The bands at 2960 cm^{-1} to 2850 cm^{-1} were assigned to aliphatic groups (CH_3, CH_2).[34] The COOH band at 1730 cm^{-1}, the CH_2 band at 1454 cm^{-1}, along with the band at 2960-2850 cm^{-1} can be attributed to lipids/aliphatic acids [13]. The band at 1240 cm^{-1} is attributable to the stretching vibration of phosphodiester backbone of nucleic acids [35]. Finally, the FT-IR spectrum revealed that HMW SKC-IOM mainly incorporates carbohydrates, protein-like structures, and lipids, a composition generally described for the so-called biopolymer fraction of natural waters [36]. In addition, Pyrolysis-GC-MS results (SI) also supported the significant presence of lipids with the identification of major peaks attributed to numerous fatty acid compounds.

The ^{13}C-NMR spectra of HMW SKC-IOM (Figure 2) showed a strong resonance peak at 72 ppm (i.e., alcohol band) associated with a well resolved band centered at 100 ppm (i.e., anomeric C), characteristic of carbohydrates [7, 14, 37]. The peak at approximately 174 ppm can be attributed to carboxyl groups present in carbohydrate moieties [11, 37]. The peak at 174 ppm can also refer to amide, as an indicator of proteins, along with the peaks in the 45-60 ppm

region corresponding to the N-alkyl linkage and amino-acid groups [11, 13]. The spectrum obtained for HMW SKC-IOM showed clear signatures of proteins with a strong signal in the 45-60 ppm region in addition to peaks at 130 and 169 ppm that corresponded to aromatic aminoacids (i.e., tyrosine). A distinct peak observed at approximately 30 ppm refers to methylene carbons present in lipids, or long straight carbon chain present in proteinaceous structures. ^{1}H-NMR results (SI) also supported the structural characteristics identified by ^{13}C-NMR.

Zeta potential (ZP) of silica and HMW SKC-IOM were clearly influenced by solution conditions (Figure 3a). Silica particles showed negative ZP throughout the entire range of ionic strength tested as previously reported [24]. The negative ZP of silica would be originated by deprotonated silanol groups at the pH of the experiments, and decreased with increasing Na^{+} concentration. The ZP of HMW SKC-IOM was also negative during the solution conditions tested and would be originated by deprotonated carboxyl groups (i.e., as described in the FTIR and ^{13}C-NMR characterization). Nevertheless, HMW SKC-IOM showed lower ZP values as compared to that of silica, and also decreased with increasing ionic strength. This low negative ZP values displayed by hydrophilic biopolymers have been previously observed (i.e., carboxyl groups is not a dominant functional group in hydrophilic biopolymers structure) [22].

The ZP values obtained were used to model energy barriers between HMW SKC-IOM and silica surface using Classic DLVO theory (Figure 3b). The value selected for Hamaker (A) constant was 4.0×10^{-21} J. This value is consistent with Hamaker constants previously reported for proteins (BSA: 4.0×10^{-21} J), river humic acid (SR-HA: 4.6×10^{-21} J), and bacterial cell (*Escherichia coli* K12 mutants having lipopolysaccharide layers: 6.5×10^{-21} J) [23, 38-40]. Briefly, energy barriers were observed between silica and HMW SKC-IOM at low ionic strength (i.e., 1, 3, and 10 mM NaCl). Nevertheless, these barriers decreased in magnitude with increasing Na^{+} concentration in solution. This decrease is associated with charge screening of

both silica and HMW SKC-IOM, resulting in reduced repulsive electrostatic forces (i.e., long-ranged forces and sensitive to ionic strength and solution composition) [30]. Interestingly, no energy barrier was observed at 30 and 100 mM NaCl, indicating the predominance of van der Waals forces (i.e., ubiquitous and not sensitive to ionic strength) over electrostatics. This simulation suggests the absence of energy barriers between silica and HMW SKC-IOM at high ionic strength. Nevertheless, classic DLVO theory does not describe interactions of organics or biological systems such as acid-base and steric forces.

As a summary of the characterization conducted on HMW SKC-IOM by Elemental Analysis, Pyrolysis-GC-MS, ^{1}H-NMR (results described in Supplementary Data section), FTIR, and ^{13}C-NMR, this isolate is defined by a high polarity and a low aromaticity (i.e., probably associated to aromatic aminoacids). The characteristics of HMW SKC-IOM are similar to those of freshwater biopolymers (i.e., as opposed to those of humic substances) [36, 41]. Briefly, this fraction mainly consists of a mixture of polysaccharides, proteins, and lipids. Also, the moderate-low negative charge of this isolate is consistent to that of freshwater biopolymers, and lower than the charge displayed by humic substances.

3.2. Nanomechanical properties of HMW SKC-IOM

The nanomechanical properties of HMW SKC-IOM were obtained through a rigorous analysis of the approaching regime of the force vs distance profiles generated between silica surface and HMW SKC-IOM-coated AFM probe at different ionic strength.

During approaching, repulsive forces following a pseudo-exponential decay were observed between silica and HMW SKC-IOM at every ionic strength tested (i.e., 1, 3, 10, 30, and 100 mM NaCl) (Figure 4a). Interestingly, classic DLVO theory (plate-sphere model) predicted no energy barrier between silica surface and HMW SKC-IOM at 30 and 100 mM NaCl solutions. The absence of energy barriers at those solution chemistries (i.e., predominance of van der Waals over electrostatic forces at 30 and 100 mM NaCl) would be translated in the occurrence

of jump in-to-contact events (i.e., gradient of attractive forces exceeding the spring constant of the cantilever) in the current AFM experimental setup [23]. Nevertheless, irrespective of solution chemistry, every recorded approaching curve showed repulsive forces (i.e., even at high ionic strength). This discrepancy between classic DLVO theory predictions and experimental data suggests the possible presence of non-DLVO forces interacting in the silica/HMW SKC-IOM system and was further investigated as follows.

Although long-ranged and high repulsive forces following a pseudo-exponential decay were observed between silica and HMW SKC-IOM in 1 mM NaCl solutions (Figure 4a), the magnitude of these forces decreased with increasing Na^+ concentration. Previous investigations have also observed a decrease in repulsive forces between surfaces and organic or biological material with increasing salt in solution [25, 42, 43]. To study these repulsive forces, two parameters were extracted from the approaching curves and statistically analyzed: a) interaction distance (i.e., interaction in contact regime between HMW SKC-IOM and silica surface occurring from the point of contact to the region of constant compliance) and b) F_0 (i.e., "Force at Contact" or pre-exponential constant described by the concept of decay length) (Figure 4a) [23, 42].

Mean interaction distances decreased with increasing salt in solution (i.e., 98.9, 69.4, 33.2, 23.9, and 21.9 nm at 1, 3, 10, 30, and 100 mM NaCl solutions, respectively) (Figure 4a, S5a, S6a-c). Similarly, F_0 (i.e., the maximum force recorded before the region of constant compliance resulting from HMW SKC-IOM interaction with silica surface) [23] also decreased with increasing ionic strength (Figure 4a, S5b), as similarly observed in previous investigations [42, 44]. Mean F_0 values were: 21.0, 14.0, 15.9, 3.3, and 1.8 nN at 1, 3, 10, 30, and 100 mM NaCl solutions, respectively. This statistical analysis clearly indicated the influence of Na^+ cations on the interaction distances and on the repulsive forces displayed by HMW SKC-IOM to silica surface. Furthermore, these results provide a quantitative evidence of the

"compression" of the force vs distance profiles as a function of solution chemistry, and also suggest a possible conformational change of HMW SKC-IOM structure. However, to elucidate the specific nature of this forces and their correlation to solution conditions, an additional analysis of the approaching curves was conducted.

Approaching curves were initially fitted using an exponential decay model to determine HMW SKC-IOM interaction force decay length (κ^{-1}) for every solution condition tested and to detect any deviation from theoretical Debye length (i.e., describing electrostatic forces as the interacting mechanism) [23, 24, 42]. Regardless of their high coefficient of determination (R^2) values, the exponential decay fit of every single force profile generated at 1, 3, 10, and 30 mM NaCl deviated from the experimental data (Figure 4b, S4a), specifically at the pseudo-exponential region. Previous investigations have documented unsuccessful attempts to accurately model approaching curves (i.e., describing organic or biological system interactions with surfaces) using an exponentially decaying function to extract their characteristic κ^{-1} parameter [23, 25, 45]. However, extended models that incorporate bi-exponential term extensions (i.e., to mathematically describe acid-base or steric interactions) have also been tested, resulting in a more detailed understanding of the dominant interacting mechanisms and physicochemical surface properties of the samples [23, 45].

Approaching curves acquired at 1, 3, 10, and 30 mM NaCl were then modeled using a bi-exponential decaying function (Figure 4b, S4a). Two regions were clearly identified during the fitting of these curves and their corresponding decay lengths were extracted; a) Region #1: starting at the point of contact between HMW SKC-IOM and silica and characterized by higher κ^{-1} values, and b) Region #2: extending <10 nm before the region of constant compliance and distinguished by lower κ^{-1} values. The decay length of Region #1 showed highly dependent on solution chemistry. The κ^{-1} values obtained for Region #1 were 12.8, 8.8, 4.4, and 2.0 nm for 1, 3, 10, and 30 mM NaCl, respectively (Figure S6d-f); while the κ^{-1} values obtained for Region

#2 were 0.74, 1.23, 0.74, and 0.2 for 1, 3, 10, and 30 mM NaCl, respectively. The values of decay length of both regions followed a trend that deviated from theoretical Debye length (Figure 5a). Specifically, κ^{-1} values of Region #1 were above Debye length, especially at 1, 3, and 10 mM NaCl. Contrariwise, the κ^{-1} values of Region #2 were significantly below Debye length at all the ionic strength range tested. The decay length at 100 mM NaCl was 0.53 nm. In addition to the classic DLVO theory prediction, these decay lengths provided another supporting evidence of the presence of non-DLVO forces interacting between HMW SKC-IOM and silica surface.

Decay lengths deviating from theoretical Debye length have been extensively documented for various organic/biological systems (e.g. bacterial cells, oocyst, or organics interactions with membranes) [23, 42, 45-47]. Those previous studies have highlighted the contribution of steric repulsive forces, which have been attributed to the polymeric nature of the tested material. The results obtained in the current study not only suggest the influence of steric interactions originating from the polymeric structure of HMW SKC-IOM, but also indicates the presence of two regions showing different nanomechanical properties. Moreover, results also suggest that the structural conformation of HMW SKC-IOM and the nanomechanical characteristics of these two regions are highly influenced by solution chemistry. To test the abovementioned hypothesis, an additional analysis of these two regions was conducted. Polymer length and polymer grafting density of HMW SKC-IOM were determined by Alexander-de Gennes model for compression of a polymer brush, as widely described in previous investigations [23, 48]. Nevertheless, Alexander-de Gennes model could not accurately fit the pseudo-exponential region of the approaching curves (Figures S4b, S7a-c). Therefore, polymer length and polymer grafting density were separately determined in Region #1 and Region #2 by Alexander-de Gennes model, following the bi-exponential approach above described (Figure S4b). The polymer lengths obtained for Region #1 were 99.6, 66.6, 26.1, and 7.0 nm for 1, 3, 10, and 30

mM NaCl, respectively (Figure S6g-i); while the polymer lengths obtained for Region #2 were 17.6, 15.1, 9.7, and 1.3 for 1, 3, 10, and 30 mM NaCl, respectively (Figure 5b). These high values of polymer length are consistent with the expected large size of HMW compounds resulting from the dialysis process (i.e., filtered through a 0.7 μm membrane and retained in a 3.5 KDa dialysis bag, section 2.2) and also observed in the LC-OCD profiles (Figure S1b). Soluble natural polysaccharides of similar length have been previously reported [49]. Furthermore, the polymer grafting density obtained for Region #1 were 6.6, 4.7, 16.0, and 41.7 (/100 nm^2) for 1, 3, 10, and 30 mM NaCl, respectively; while for Region #2 were 27.1, 34.7, 41.1, and 128 (/100 nm^2) for 1, 3, 10, and 30 mM NaCl, respectively (Figure 6a). Polymer length and polymer grafting density could not be accurately determined at 100 mM NaCl due to high scatter in the experimental data. These results indicate that mean length of HMW SKC-IOM polymer brush in both Regions #1 and #2 follow a decreasing trend (i.e., decreasing thickness) with increasing salt in solution. Conversely, the mean polymer grafting density of both regions increased with increasing NaCl concentration. Previous AFM studies investigating the characteristics of polymeric structures have reported similar trends. For instance, the conformation and length of extra cellular polymers on bacteria surface have been observed to highly respond to ionic strength and pH [50, 51]. Polyethylene Glycol (PEG) brushes anchored on a gold ring have been reported to extend or collapse under good (PBS) or poor (10% 2-propanol) solvent conditions (i.e., change in conformation), respectively [52]. In this latter study, surface functionalities were suggested to play a significant role in this change of conformation; where the forces recorded decayed exponentially and were described as sterically repulsive. Therefore, the decrease observed in HMW SKC-IOM polymer length with increasing electrolyte in solution would be a response to poor solvent conditions. Indeed, the high values of polymer length at low ionic strength suggest fully extended polymeric structures of high polarity (i.e., highly interacting with water molecules). This polarity would be

originated from the high aliphaticity, low aromaticity, high content of alcoholic groups, and moderate negative charge of HMW SKC-IOM molecules (i.e., as observed in ^{13}C-NMR, FTIR, ^{1}H-NMR, and zeta potential measurements). However, increasing Na^{+} indifferent cations (i.e., weak outer-sphere complexation, increasing charge screening [53, 54]) in solution would influence HMW SKC-IOM intermolecular and intramolecular interactions [55, 56]. In addition to polysaccharides, Pyrolysis GC-MS, ^{13}C-NMR, FTIR, and ^{1}H-NMR characterization also indicated a significant presence of proteins and lipids in HMW SKC-IOM structure. Proteins and lipids are expected to show considerably less polarity than polysaccharides [57], and would highly rely on deprotonated carboxyl groups (i.e., providing negative charge) for interacting with the surrounding solvent. Consequently, increasing electrolyte in solution would result in HMW SKC-IOM conformational changes where lipids and proteins would be structurally rearranged to interact less with water molecules, responding to entropic changes. Consequently, this compression of HMW SKC-IOM structures would be reflected in an increase in polymer grafting density, as consistently observed in Figure 6a.

Interestingly, a comprehensive AFM study conducting indentation on PEG brushes also observed two regions of different nanomechanical properties [48]. Similarly to the current investigation, the mechanical response of these PEG brushes to compression (i.e., analyzed in approaching curves) evidenced regions of different thickness and elastic modulus: a) Region #1: located farther from the substrate and showing extended polymeric chains, and b) Region #2: located within the last few nanometers above the substrate and presenting constraint chains (i.e., stiffer film). To obtain a more detailed understanding of HMW SKC-IOM conformational change with solution conditions, compressibility was determined based on Alexander-de Gennes model [58]. As expected, with increasing electrolyte concentration, the polymer grafting density of Regions #1 and #2 also increased, thus resulting in higher compressibility of the brush layers (Figure 6a-b). Also, polymer grafting density and compressibility in Region

#2 were higher than in Region #1 throughout the entire ionic strength range tested, indicating a direct correlation. These trends in polymer length, polymer grafting density, and compressibility as a function of solution chemistry would be explained as follows. The HMW SKC-IOM brush layers in both Region #1 and #2 showed increasing resistance to compression with: a) increasing ionic strength, and b) as the colloidal probe approaches to the silica surface. These increasing (exponential) repulsive forces are the result of a decrease in entropy of the confined HMW SKC-IOM polymeric chains. Therefore, a decrease in HMW SKC-IOM polymer length would directly lead to an increased polymer grafting density and to increase in compressibility, as observed in the current results.

The interaction forces between HMW SKC-IOM and silica surface have been mathematically modeled using a bi-exponential model. This model suggested the presence of two regions of different nanomechanical properties, also highly impacted by solution chemistry. The hypothesis of a two-region system would be supported by the characteristics of HMW SKC-IOM. According to the characterization results, this fraction is a heterogeneous mix mainly composed of large polysaccharide-like and protein-like compounds of different properties and structures. Therefore, polysaccharides and proteins would also be expected to display different nanomechanical properties that could be modelled as a two-component system, resulting in different decay lengths, polymer lengths, and compressibility.

4. Conclusions: Environmental Implications

A detailed characterization of algal organic matter (i.e., including mechanical properties at the nanoscale) represents a fundamental steppingstone for understanding algal biopolymers interactions with surfaces, which has strong implications for the investigation of membrane fouling in desalination systems. In the current study, the HMW compounds of SKC-IOM were selected as model AOM. The environmental relevance of the selection of this organic fraction is based on the following: a) HMW organic compounds (i.e., of surface water or AOM origin)

have been widely investigated and proposed as highly influential fractions inducing fouling on polymeric and ceramic membranes [59-61], and b) IOM represent a common environmental scenario occurring in aging algae blooms: lysis of cells and intracellular organic matter release. A rigorous characterization of HMW SKC-IOM indicated a fraction of high polarity, consisting mainly of polysaccharides, proteins, and lipids. AFM provided crucial information at a nanoscale spatial resolution, specifically nanomechanical properties. HMW SKC-IOM showed highly responsive to solution chemistry: fully extended chains at low ionic strength, and compressing structures with increasing electrolyte concentration in solution. These results suggest the influence of steric interactions originating from the polymeric structure of HMW SKC-IOM, and indicate the presence of two regions of different nanomechanical properties also highly impacted by solution chemistry. The current investigation has successfully applied models of polymer physics to describe the complex polymeric nature of an algal fraction at different solution conditions. In addition, results from this investigation would contribute to understand biopolymers conformational changes with solution conditions (e.g., seawater, brine, or freshwater), and how these conformational changes would influence biopolymers interactions with surfaces (e.g., filtration membranes). Finally, the detailed methodology presented in this investigation to study the polymeric nature of AOM at different solution chemistries can be potentially extended to other organic compounds of environmental relevance.

Acknowledgements

The authors are grateful to the funding from King Abdullah University of Science and Technology (KAUST).

Supplementary Data

Characterization protocols of the High Molecular Weight compounds of SKC-IOM. Elemental analysis, LC-OCD profiles, Pyrolysis GC-MS pyrochromatogram, and ^{1}H-NMR spectra of HMW SKC-IOM. Representative force vs distance profiles and analysis of interaction distances and F_o during approaching regime at different solution conditions. Supplementary data associated with this article can be found, in the online version, at:

References

[1] WHO, UNICEF, W.S.S.C. Council, W.U.J.W.S.S.M. Programme, Global water supply and sanitation assessment 2000 report, World Health Organization2000.
[2] C. Fritzmann, J. Löwenberg, T. Wintgens, T. Melin, State-of-the-art of reverse osmosis desalination, Desalination, 216 (2007) 1-76.
[3] L.O. Villacorte, S.A.A. Tabatabai, D.M. Anderson, G.L. Amy, J.C. Schippers, M.D. Kennedy, Seawater reverse osmosis desalination and (harmful) algal blooms, Desalination, 360 (2015) 61-80.
[4] D.A. Caron, M.-È. Garneau, E. Seubert, M.D.A. Howard, L. Darjany, A. Schnetzer, I. Cetinić, G. Filteau, P. Lauri, B. Jones, S. Trussell, Harmful algae and their potential impacts on desalination operations off southern California, Water Res., 44 (2010) 385-416.
[5] M.L. Richlen, S.L. Morton, E.A. Jamali, A. Rajan, D.M. Anderson, The catastrophic 2008–2009 red tide in the Arabian gulf region, with observations on the identification and phylogeny of the fish-killing dinoflagellate Cochlodinium polykrikoides, Harmful Algae, 9 (2010) 163-172.
[6] S.E.H. Niven, P.E. Kepkay, A. Boraie, Colloidal organic carbon and colloidal 234Th dynamics during a coastal phytoplankton bloom, Deep-Sea Res. Part II Top. Stud. Oceanogr., 42 (1995) 257-273.
[7] M.L. Nguyen, P. Westerhoff, L. Baker, Q. Hu, M. Esparza-Soto, M. Sommerfeld, Characteristics and reactivity of algae-produced dissolved organic carbon, J. Environ. Eng., 131 (2005) 1574-1582.
[8] M. Pivokonsky, J. Safarikova, M. Baresova, L. Pivokonska, I. Kopecka, A comparison of the character of algal extracellular versus cellular organic matter produced by cyanobacterium, diatom and green alga, Water Res., 51 (2014) 37-46.
[9] W. Huang, H. Chu, B. Dong, Characteristics of algogenic organic matter generated under different nutrient conditions and subsequent impact on microfiltration membrane fouling, Desalination, 293 (2012) 104-111.
[10] L.O. Villacorte, Y. Ekowati, T.R. Neu, J.M. Kleijn, H. Winters, G. Amy, J.C. Schippers, M.D. Kennedy, Characterisation of algal organic matter produced by bloom-forming marine and freshwater algae, Water Res., 73 (2015) 216-230.
[11] J.I. Hedges, J.A. Baldock, Y. Gélinas, C. Lee, M.L. Peterson, S.G. Wakeham, The biochemical and elemental compositions of marine plankton: A NMR perspective, Mar. Chem., 78 (2002) 47-63.

[12] D.J. Repeta, T.M. Quan, L.I. Aluwihare, A. Accardi, Chemical characterization of high molecular weight dissolved organic matter in fresh and marine waters, Geochim. Cosmochim. Acta, 66 (2002) 955-962.
[13] J.A. Leenheer, Systematic approaches to comprehensive analyses of natural organic matter, Ann. Environ. Sci., 3 (2009) 1-130.
[14] A.H. Gillam, M.A. Wilson, Pyrolysis-GC-MS and NMR studies of dissolved seawater humic substances and isolates of a marine diatom, Org. Geochem., 8 (1985) 15-25.
[15] D.L. Widrig, K.A. Gray, K.S. McAuliffe, Removal of algal-derived organic material by preozonation and coagulation: Monitoring changes in organic quality by pyrolysis-GC-MS, Water Res., 30 (1996) 2621-2632.
[16] J. Fang, X. Yang, J. Ma, C. Shang, Q. Zhao, Characterization of algal organic matter and formation of DBPs from chlor(am)ination, Water Res., 44 (2010) 5897-5906.
[17] Y. Zhang, J. Tian, H. Liang, J. Nan, Z. Chen, G. Li, Chemical cleaning of fouled PVC membrane during ultrafiltration of algal-rich water, J. Environ. Sci., 23 (2011) 529-536.
[18] E.V. Sokolova, E.A. Chusovitin, A.O. Barabanova, S.A. Balagan, N.G. Galkin, I.M. Yermak, Atomic force microscopy imaging of carrageenans from red algae of Gigartinaceae and Tichocarpaceae families, Carbohydr. Polym., 93 (2013) 458-465.
[19] J.A. Callow, S.A. Crawford, M.J. Higgins, P. Mulvaney, R. Wetherbee, The application of atomic force microscopy to topographical studies and force measurements on the secreted adhesive of the green alga Enteromorpha, Planta, 211 (2000) 641-647.
[20] L. Shen, H. Xu, X. Guo, P. Wu, Oceanography of Skeletonema costatum harmful algal blooms in the East China Sea using MODIS and QuickSCAT satellite data, J. Appl. Remote Sens., 6 (2012) 063529-063521-063529-063518.
[21] L. Dramas, Ceramic Ultrafiltration of Marine Algal Solutions: A Comprehensive Study, Environmental Science and Engineering Program, King Abdullah University of Science and Technology Kingdom of Saudi Arabia, 2014, pp. 253.
[22] L. Gutierrez, C. Aubry, M. Cornejo, J.-P. Croue, Citrate-Coated Silver Nanoparticles Interactions with Effluent Organic Matter: Influence of Capping Agent and Solution Conditions, Langmuir, 31 (2015) 8865-8872.
[23] H.J. Butt, B. Cappella, M. Kappl, Force measurements with the atomic force microscope: Technique, interpretation and applications, Surf. Sci. Rep., 59 (2005) 1-152.
[24] L. Gutierrez, T.H. Nguyen, Interactions between Rotavirus and Suwannee River Organic Matter: Aggregation, Deposition, and Adhesion Force Measurement, Environ. Sci. Technol., 46 (2012) 8705-8713.
[25] C. Aubry, L. Gutierrez, J.P. Croue, Coating of AFM probes with aquatic humic and non-humic NOM to study their adhesion properties, Water Res., 47 (2013) 3109-3119.
[26] L. Gutierrez, T.H. Nguyen, Interactions between rotavirus and natural organic matter isolates with different physicochemical characteristics, Langmuir, 29 (2013) 14460-14468.
[27] L. Gutierrez, C. Aubry, R. Valladares Linares, J.-P. Croue, Natural organic matter interactions with polyamide and polysulfone membranes: Formation of conditioning film, Colloids Surf., A, 477 (2015) 1-8.
[28] A.W. Chassé, T. Ohno, S.R. Higgins, A. Amirbahman, N. Yildirim, T.B. Parr, Chemical Force Spectroscopy Evidence Supporting the Layer-by-Layer Model of Organic Matter Binding to Iron (oxy)Hydroxide Mineral Surfaces, Environ. Sci. Technol., 49 (2015) 9733-9741.
[29] S.K. Lower, C.J. Tadanier, M.F. Hochella, Measuring interfacial and adhesion forces between bacteria and mineral surfaces with biological force microscopy, Geochim. Cosmochim. Acta, 64 (2000) 3133-3139.
[30] J.N. Israelachvili, Intermolecular and Surface Forces: Revised Third Edition, Elsevier Science2011.
[31] F.P. Gordesli, N.I. Abu-Lail, The Role of Growth Temperature in the Adhesion and Mechanics of Pathogenic L. monocytogenes: An AFM Study, Langmuir, 28 (2012) 1360-1373.

[32] J. Gregory, Approximate expressions for retarded van der waals interaction, Journal of Colloid And Interface Science, 83 (1981) 138-145.
[33] R. Hogg, T.W. Healy, Fuersten.Dw, MUTUAL COAGULATION OF COLLOIDAL DISPERSIONS, Transactions of the Faraday Society, 62 (1966) 1638-&.
[34] M. Igisu, Y. Ueno, M. Shimojima, S. Nakashima, S.M. Awramik, H. Ohta, S. Maruyama, Micro-FTIR spectroscopic signatures of Bacterial lipids in Proterozoic microfossils, Precambrian Res., 173 (2009) 19-26.
[35] D. Naumann, C.P. Schultz, D. Helm, What can infrared spectroscopy tell us about the structure and composition of intact bacterial cells?, 1996.
[36] J.A. Leenheer, J.P. Croué, Characterizing aquatic dissolved organic matter, Environ. Sci. Technol., 37 (2003) 18A-26A.
[37] R. Benner, J.D. Pakulski, M. McCarthy, J.I. Hedges, P.G. Hatcher, Bulk chemical characteristics of dissolved organic matter in the ocean, Science, 255 (1992) 1561-1564.
[38] S.E. Mylon, K.L. Chen, M. Elimelech, Influence of natural organic matter and ionic composition on the kinetics and structure of hematite colloid aggregation: Implications to iron depletion in estuaries, Langmuir, 20 (2004) 9000-9006.
[39] A.J. de Kerchove, M. Elimelech, Relevance of electrokinetic theory for "soft" particles to bacterial cells: Implications for bacterial adhesion, Langmuir, 21 (2005) 6462-6472.
[40] Z.A. Kuznar, M. Elimelech, Role of surface proteins in the deposition kinetics of Cryptosporidium parvum oocysts, Langmuir, 21 (2005) 710-716.
[41] J.-P. Croué, Isolation of Humic and Non-Humic NOM Fractions: Structural Characterization, Environ. Monit. Assess., 92 (2004) 193-207.
[42] T.L. Byrd, J.Y. Walz, Interaction force profiles between Cryptosporidium parvum oocysts and silica surfaces, Environ. Sci. Technol., 39 (2005) 9574-9582.
[43] J.J. Valle-Delgado, J.A. Molina-Bolévair, F. Galisteo-González, M.J. Gálvez-Riuz, A. Feiler, M.W. Rutland, Interaction forces between BSA layers adsorbed on silica surfaces measured with an atomic force microscope, J. Phys. Chem. B, 108 (2004) 5365-5371.
[44] M. Finessi, P. Sinha, I.n. Szilágyi, I. Popa, P. Maroni, M. Borkovec, Charge Reversal of Sulfate Latex Particles by Adsorbed Linear Poly(ethylene imine) Probed by Multiparticle Colloidal Probe Technique, J. Phys. Chem. B, 115 (2011) 9098-9105.
[45] L.S. Dorobantu, S. Bhattacharjee, J.M. Foght, M.R. Gray, Analysis of Force Interactions between AFM Tips and Hydrophobic Bacteria Using DLVO Theory, Langmuir, 25 (2009) 6968-6976.
[46] S. Kang, M. Elimelech, Bioinspired Single Bacterial Cell Force Spectroscopy, Langmuir, 25 (2009) 9656-9659.
[47] A. Asatekin, A. Menniti, S.T. Kang, M. Elimelech, E. Morgenroth, A.M. Mayes, Antifouling nanofiltration membranes for membrane bioreactors from self-assembling graft copolymers, J. Membr. Sci., 285 (2006) 81-89.
[48] G. Stan, F.W. DelRio, R.I. MacCuspie, R.F. Cook, Nanomechanical Properties of Polyethylene Glycol Brushes on Gold Substrates, J. Phys. Chem. B, 116 (2012) 3138-3147.
[49] S. Dumitriu, Polysaccharides: Structural Diversity and Functional Versatility, Second Edition, CRC Press2004.
[50] T.A. Camesano, B.E. Logan, Probing Bacterial Electrosteric Interactions Using Atomic Force Microscopy, Environ. Sci. Technol., 34 (2000) 3354-3362.
[51] N.I. Abu-Lail, T.A. Camesano, Elasticity of Pseudomonas putida KT2442 Surface Polymers Probed with Single-Molecule Force Microscopy, Langmuir, 18 (2002) 4071-4081.
[52] R.Y.H. Lim, J. Deng, Interaction Forces and Reversible Collapse of a Polymer Brush-Gated Nanopore, ACS Nano, 3 (2009) 2911-2918.
[53] A.G. Kalinichev, E. Iskrenova-Tchoukova, W.-Y. Ahn, M.M. Clark, R.J. Kirkpatrick, Effects of Ca2+ on supramolecular aggregation of natural organic matter in aqueous solutions: A comparison of molecular modeling approaches, Geoderma, 169 (2011) 27-32.

[54] A.G. Kalinichev, R.J. Kirkpatrick, Molecular dynamics simulation of cationic complexation with natural organic matter, Eur. J. Soil Sci., 58 (2007) 909-917.
[55] M.J. Avena, A.W.P. Vermeer, L.K. Koopal, Volume and structure of humic acids studied by viscometry pH and electrolyte concentration effects, Colloids Surf., A, 151 (1999) 213-224.
[56] J.R. Lead, K.J. Wilkinson, K. Starchev, S. Canonica, J. Buffle, Determination of diffusion coefficients of humic substances by fluorescence correlation spectroscopy: Role of solution conditions, Environ. Sci. Technol., 34 (2000) 1365-1369.
[57] A. Tiraferri, Y. Kang, E.P. Giannelis, M. Elimelech, Superhydrophilic Thin-Film Composite Forward Osmosis Membranes for Organic Fouling Control: Fouling Behavior and Antifouling Mechanisms, Environ. Sci. Technol., 46 (2012) 11135-11144.
[58] N. Guz, M. Dokukin, V. Kalaparthi, I. Sokolov, If Cell Mechanics Can Be Described by Elastic Modulus: Study of Different Models and Probes Used in Indentation Experiments, Biophys. J., 107 (2014) 564-575.
[59] N. Lee, G. Amy, J.-P. Croué, H. Buisson, Identification and understanding of fouling in low-pressure membrane (MF/UF) filtration by natural organic matter (NOM), Water Res., 38 (2004) 4511-4523.
[60] N. Lee, G. Amy, J.P. Croue, Low-pressure membrane (MF/UF) fouling associated with allochthonous versus autochthonous natural organic matter, Water Res., 40 (2006) 2357-2368.
[61] X. Zhang, L. Fan, F.A. Roddick, Understanding the fouling of a ceramic microfiltration membrane caused by algal organic matter released from Microcystis aeruginosa, J. Membr. Sci., 447 (2013) 362-368.

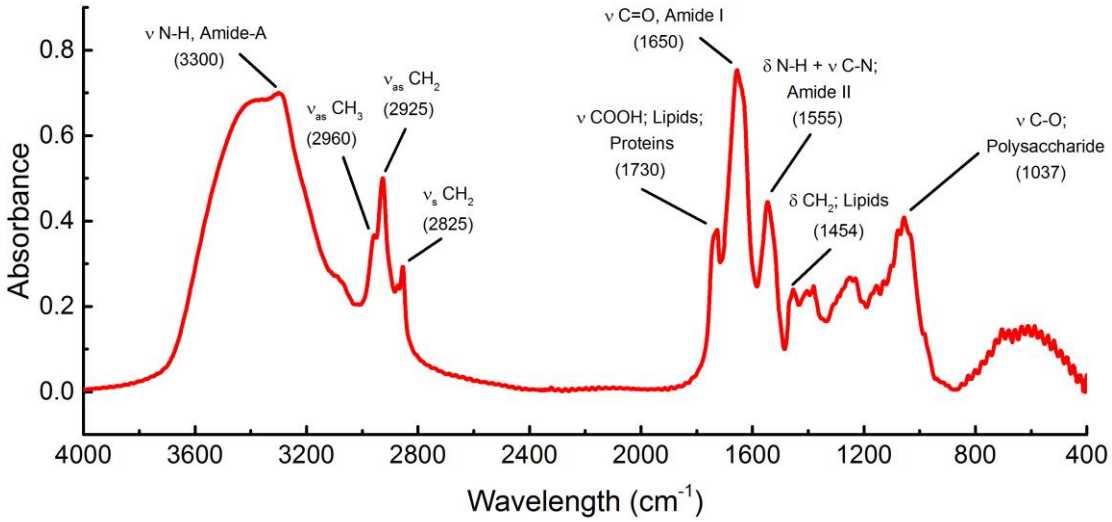

Figure 1. FTIR spectra of HMW SKC-IOM isolate.

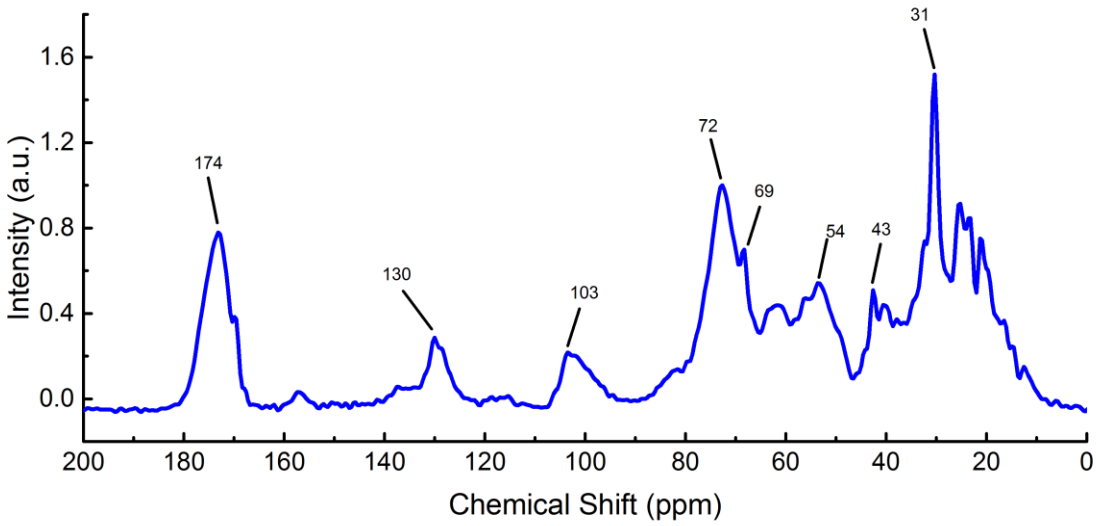

Figure 2. ^{13}C-NMR spectra of HMW SKC-IOM isolate.

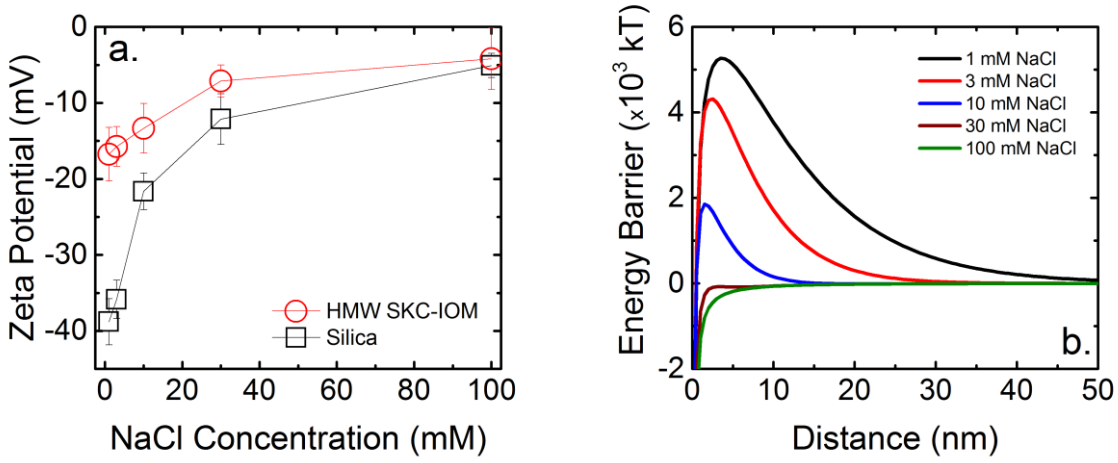

Figure 3. a) Zeta potential of silica particles (ϕ:1.6 μm) and HMW SKC-IOM-coated silica particles in solutions of different ionic strength. b) Classic DLVO simulations of energy barriers between HMW SKC-IOM-coated AFM colloidal probe (ϕ:20 μm) and silica surface (sphere-plate model).

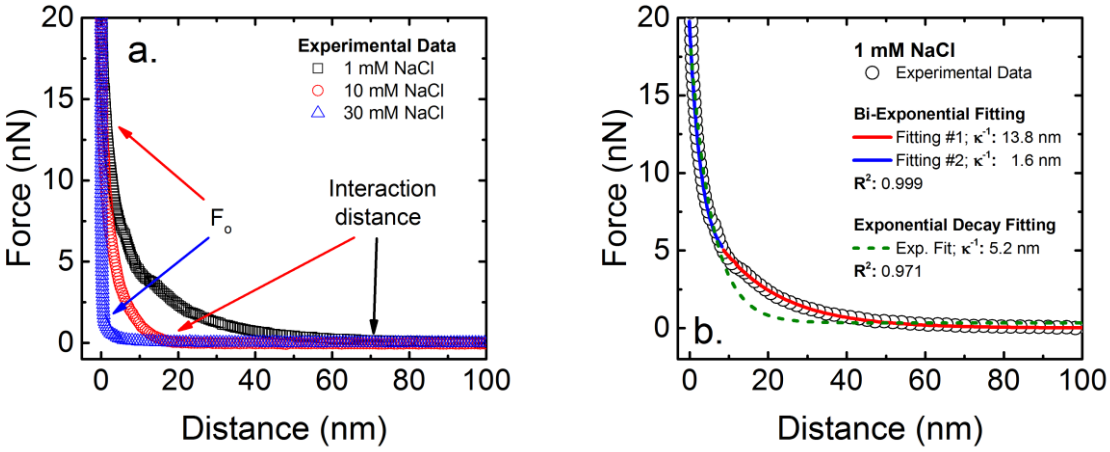

Figure 4. Representative force vs distance profiles at approaching regime. a) These curves generated at 1, 10, and 30 mM NaCl illustrate the change in F_0 and interaction distances with ionic strength. b) This curve acquired in 1 mM NaCl was fitted using exponential decay (green dotted line) and bi-exponential decay (red and blue solid lines). The latter model suggests the presence of 2 regions of different properties.

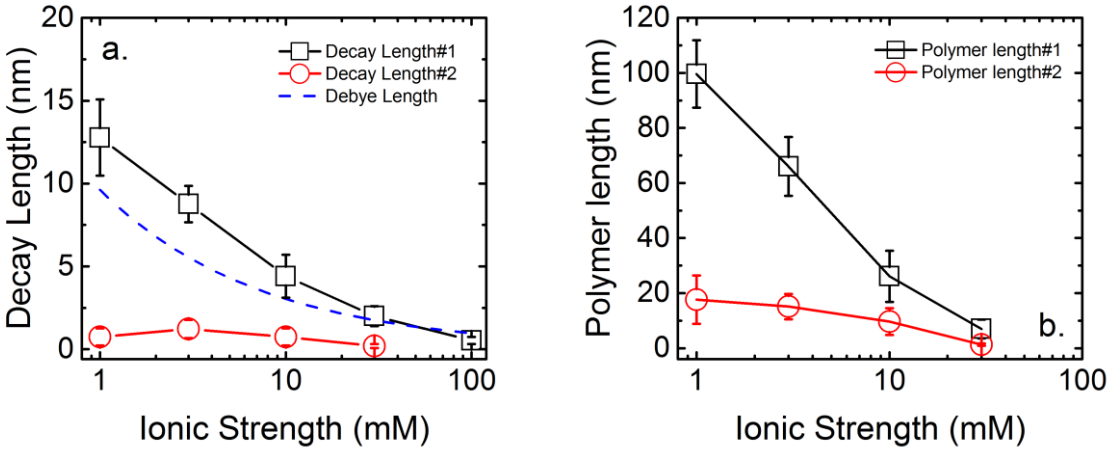

Figure 5. Mean a) decay length and b) polymer length were calculated for the two regions of different nanomechanical properties. Polymer length was determined based on Alexander-de Gennes model.

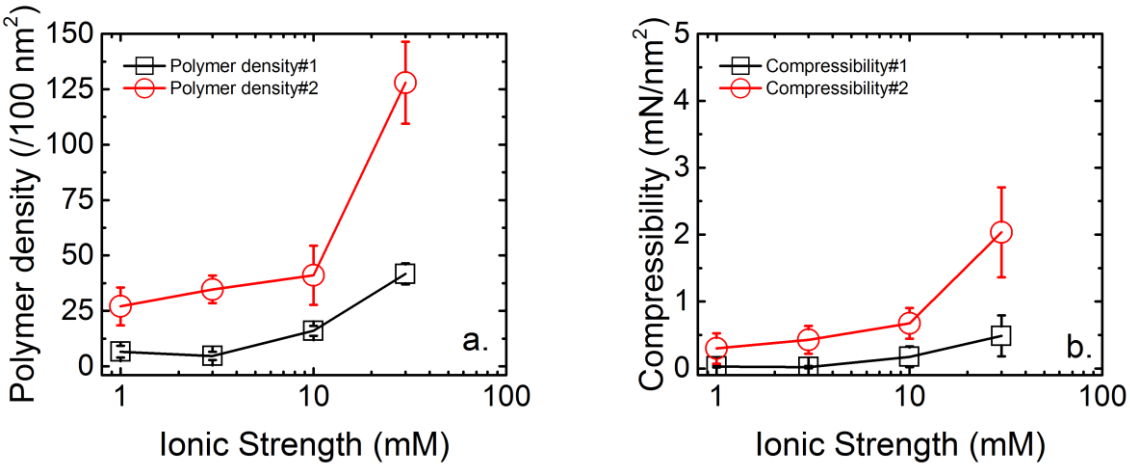

Figure 6. a) Polymer grafting density and b) compressibility calculated for the 2 regions of different nanomechanical properties. Polymer grafting density and compressibility were determined based on Alexander-de Gennes model.